Received: 18 May 2022 | Accepted: 16 June 2022

DOI: 10.1111/bpa.13108

RESEARCH ARTICLE

Brain Pathology

TREM2-induced activation of microglia contributes to synaptic integrity in cognitively intact aged individuals with Alzheimer's neuropathology

Anna Fracassi[1] | **Michela Marcatti**[1] | **Batbayar Tumurbaatar**[1] | **Randall Woltjer**[2] | **Sandra Moreno**[3] | **Giulio Taglialatela**[1]

[1]Mitchell Center for Neurodegenerative Diseases, Department of Neurology, University of Texas Medical Branch (UTMB), Galveston, Texas, USA

[2]Department of Pathology, Oregon Health and Science University, Portland, Oregon, USA

[3]Department of Science, LIME, University Roma Tre, Rome, Italy

Correspondence
Giulio Taglialatela, Mitchell Center for Neurodegenerative Diseases, Department of Neurology, University of Texas Medical Branch (UTMB), 301 University Blvd, Route 0539, Galveston, TX 77550, USA.
Email: gtaglial@utmb.edu

Funding information
NIH/NIA, Grant/Award Numbers: R01AG060718, R01AG069433, P30AG008017; Excellence Departments, MIUR, Grant/Award Number: L.232/2016; Robert J. and Helen C. Kleberg Foundation

Abstract

The existence of individuals who remain cognitively intact despite presenting histopathological signs of Alzheimer's disease (AD), here referred to as "Nondemented with AD neuropathology" (NDAN), suggests that some mechanisms are triggered to resist cognitive impairment. Exposed phosphatidylserine (ePS) represents a neuronal "eat-me" signal involved in microglial-mediated phagocytosis of damaged synapses. A possible mediator of this process is TREM2, a microglial surface receptor activated by ligands including PS. Based on TREM2 role in the scavenging function of microglia, we hypothesize that an efficient microglial phagocytosis of damaged synapses underlies synaptic resilience in NDAN, thus protecting from memory deficits. Using immunofluorescence microscopy, we performed a comparative study of human post-mortem frontal cortices of aged-matched, AD and NDAN individuals. We studied the distribution of activated microglia (IBA1, $IBA1^{+}/CD68^{+}$ cells) and phagocytic microglia-related proteins (TREM2, DAP12), demonstrating higher microglial activation and TREM2 expression in NDAN versus AD. A study of the preservation of synapses around plaques, assessed using MAP2 and βIII tubulin as dendritic and axonal markers, respectively, and PSD95 as a postsynaptic marker, revealed preserved axonal/dendritic structure around plaques in NDAN versus AD. Moreover, high levels of PSD95 around NDAN plaques and the colocalization of PSD95 with CD68 indicated a prompt removal of damaged synapses by phagocytic microglia. Furthermore, Annexin V assay on aged-matched, AD and NDAN individuals synaptosomes revealed increased levels of ePS in NDAN, confirming damaged synapses engulfment. Our results suggest a higher efficiency of TREM2-induced phagocytic microglia in removing damaged synapses, underlying synaptic resilience in NDAN individuals.

KEYWORDS
Alzheimer's disease, microglia, phosphatidylserine, resilience, synapses, TREM2

1 | INTRODUCTION

Alzheimer's disease (AD) is a progressive neurodegenerative disorder and the most common form of dementia, currently affecting more than 44 million people worldwide [1]. From a neuropathological point of view, AD responds to a specific criterion, that is the presence of two distinct histopathological markers: extracellular

deposition of β-amyloid (Aβ) in the form of diffuse and neuritic plaques, and intraneuronal neurofibrillary tangles (NFTs) formed by aggregates of tau protein [2]. However, the correlation between the accumulation of Aβ and NFTs with the progression of dementia has been questioned in the past decade by the emergence of a particular cohort of individuals recently classified as $A^+T^+N^-$, where "A" refers to the value of a Aβ biomarker (amyloid PET or CSF $A\beta_{42}$); "T," the value of a tau biomarker (CSF phospho tau, or tau PET); and "N," biomarkers of neurodegeneration or neuronal injury ([^{18}F]-fluorodeoxyglucose–PET, structural MRI, or CSF total tau) [2]. These individuals, here referred to as "Non-Demented with AD Neuropathology" (NDAN), despite presenting Aβ plaques and NFTs, most comparable to fully symptomatic AD patients, do not exhibit changes in cognitive functions, thus remaining cognitively intact suggesting that some unknown mechanisms are triggered to allow the preservation of cognitive functions in these individuals. We previously reported that synapses of NDAN subjects display a unique proteomic profile and miRNA regulation [3, 4] and are resistant to the detrimental binding of Aβ and Tau oligomers [5, 6]. Furthermore, NDAN individuals present an increased number of neural stem cells in the hippocampus [7] and preserved antioxidant response [8] that are associated with resistance to Aβ and Tau toxicity. Among the several mechanisms underlying AD pathology, synaptic dysfunction and loss have been identified as major contributors to the pathogenesis [9]. Initially the damage occurs to synapses that are in the proximity of plaques on passing axons [10]. This is evident from the consistent presence of dystrophic synapses in and around plaques [11]. It is well established that microglia attracted to plaques play an extremely important role in the engulfment of damaged synapses, thus providing protection from greater damage [10]. Therefore, the level of synaptic health is strictly related to the efficiency of microglial phagocytosis: if microglia promptly remove Aβ-injured synapses, the damage may be restricted to the immediate vicinity of the plaque. In this context, exposed phosphatidylserine (ePS) represents a neuronal "eat-me" signal on injured synapses and it is involved in microglial-mediated pruning and removal of damaged synapses [12]. A possible candidate mediator of this process is the Triggering Receptor Expressed in Myeloid cells 2 (TREM2), recently identified as an AD risk factor [13–17]. TREM2 acts as a cell surface receptor on microglia, and it has been demonstrated to bind nanomolar concentration of Aβ and ApoE [18], as well as aminophospholipids like PS [19]. TREM2 binding initiates signal transduction pathways that promote microglial chemotaxis, phagocytosis, survival, and proliferation [20], particularly through downstream activating adaptor protein DAP12 [21, 22]. This confers phagocytic signature to the microglia.

Based on the role of TREM2 in triggering the scavenging function of activated microglia [23], we hypothesized that an efficient TREM2-driven microglial phagocytosis underlies structural integrity and functionality of synapses in NDAN, thus protecting from ensuing cognitive deficits. Furthermore, an efficient recognition of the ePS by TREM2 in NDAN individuals might underlie a highly competent removal of damaged synapses through synaptic pruning. To test our hypothesis, we performed a comparative study of human post-mortem frontal cortices (FC) of normally aged individuals (here referred also as controls), AD patients and NDAN subjects, focusing on the expression of activated microglia and microglia-related proteins in relation to Aβ plaques. Using immunofluorescence (IF) techniques, we analyzed the activation of microglia elicited by the presence of Aβ plaques studying the expression and distribution of microglial key markers, such as IBA1, CD68, TREM2, and DAP12. Furthermore, to give solid foundation to our hypothesis and to test the efficacy of microglia in the engulfment of debris and damaged synapses, we looked for the presence of postsynaptic elements (PSD95) in the microglial lysosomes (CD68). Moreover, we performed a study of the preservation of synapses around plaques using Microtubule Associated Protein 2 (MAP2) and βIII tubulin as dendritic and axonal markers, respectively. Finally, we evaluated the levels of ePS in synaptosomes isolated from normally aged, AD, and NDAN individuals using flow cytometry Annexin V (ANXV) assay and super resolution microscopy.

Understanding the molecular and cellular mechanisms underlying resilience will reveal new targets for the development of innovative strategies, based on inducing cognitive resilience in individuals affected by AD neuropathology.

2 | RESULTS

2.1 | NDAN patients show higher levels of IBA1 and TREM2 around Aβ plaques

Given the involvement of microglia in neuroinflammation and the scavenging function of activated microglia in the clearance of Aβ deposits and damaged synapses, we determined the expression and localization of specific microglial markers in relation to senile plaques. Firstly, by using IF, we investigated the expression and distribution of the most common microglial marker, IBA1 [24, 25] in combination with Aβ. We detected significantly higher levels of IBA1 in AD patients as compared to aged-matched individuals, and significantly increased level of the same marker in NDAN subjects (Figure 1A–C). When quantitatively analyzed, IBA1 immunoreactivity levels, appeared significantly higher in NDAN as compared to AD and control individuals, both in terms of integrated density of fluorescence (Figure 1B) and number of $IBA1^+$ cells over the total number of cells around plaques (Figure 1C). Noteworthy, in the proximity of Aβ plaques, NDAN

subjects showed a significant increase of IBA1$^+$ cells (white arrowheads) near amyloid deposits (Figure 2A).

To exclude the presence of infiltrating myeloid cells, we performed double staining of IBA1 in combination with CD11a as a peripheral marker (Figure S1). IF imaging of microglia in AD and NDAN FC consistently showed that microglia (IBA1$^+$) near plaques did not associate with CD11a showing that plaque-associated

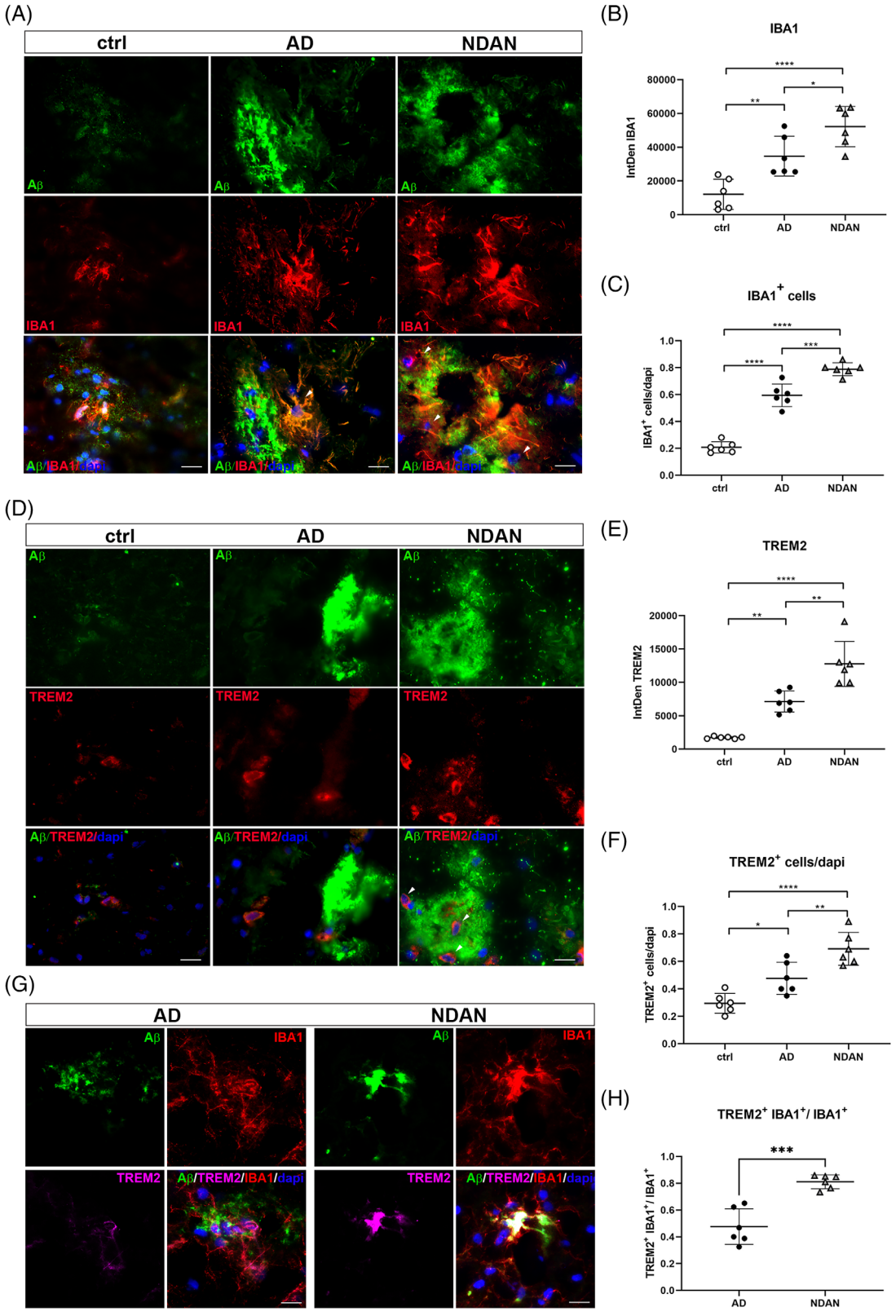

FIGURE 1 Legend on next page.

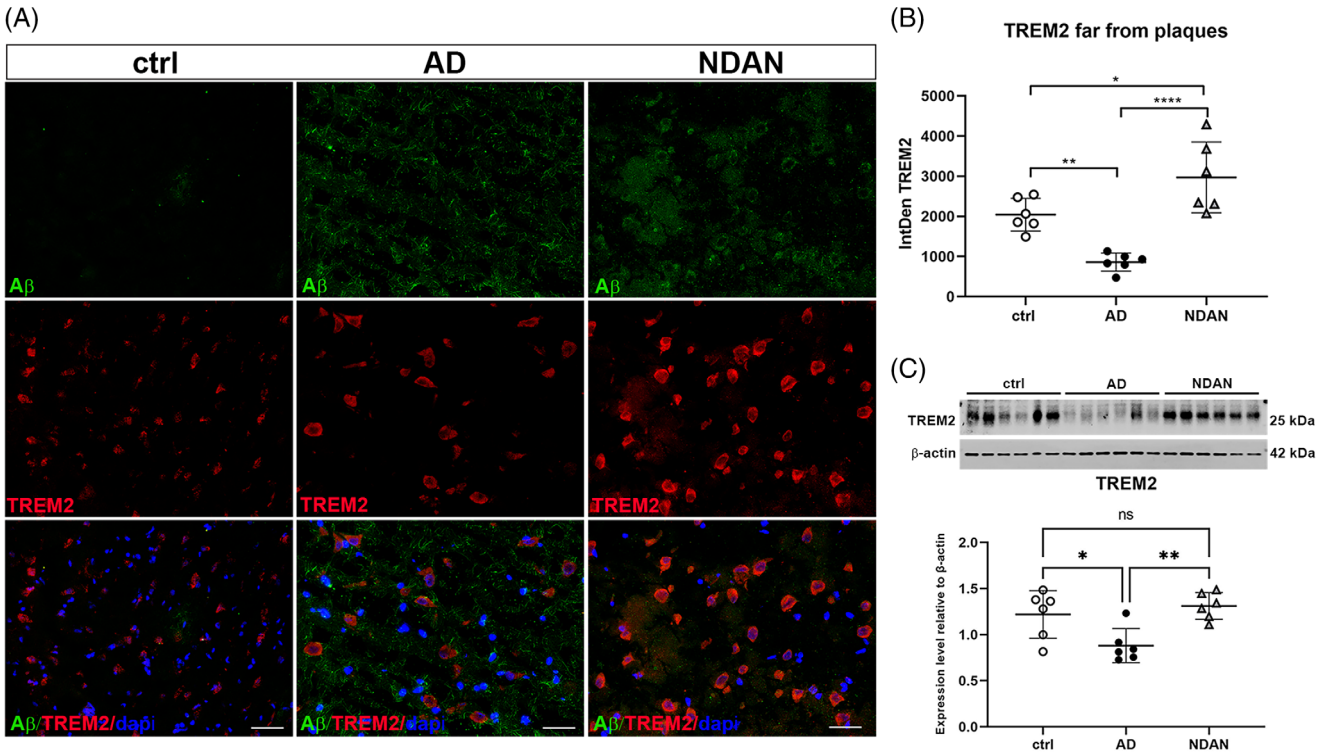

FIGURE 2 Expression and distribution of TREM2 far from plaques in age-matched, Alzheimer's disease (AD), and Nondemented with AD neuropathology (NDAN) subjects. (A,B) Representative images of double immunofluorescence (IF) staining of TREM2 (red) and β-amyloid (Aβ) (green) and quantitative analyses showing higher overall distribution of TREM2 in NDAN individuals as compared to AD and controls subjects even far from Aβ plaques. AD patients show significantly low levels of TREM2 as respect to controls and NDAN. Scale bar 30 μm. (C) WB analyses of human frontal cortices confirming the significantly decreased levels of TREM2 in AD patients as respect to aged-matched and NDAN individuals. Statistical analyses were made using one-way analysis of variance, following Tukey's multiple-comparisons test. Values are expressed as the mean ± SD. (B) Ctrl versus AD ** $p = 0.0076$; AD versus NDAN **** $p < 0.0001$; ctrl versus NDAN * $p = 0.0345$. (C) Ctrl versus AD $p = 0.0270$; AD versus NDAN * $p = 0.0056$; ctrl versus NDAN $p = 0.7168$

myeloid cells are microglia and not circulating monocytes/macrophages. Occasionally CD11a $^{+}$ IBA1^{-} cells were found near plaques meaning they were not of myeloid lineage as described also by [26].

In view of TREM2 as a strong risk factor for AD in humans and as a critical regulator of microglial activity in mouse model of AD [13–17, 20, 27], we quantitatively analyzed the expression and distribution of TREM2 in relation to Aβ plaques by using IF techniques in post-mortem brain of control subjects, AD patients, and NDAN individuals (Figure 1D–F). Similarly to what observed for IBA1 immunoreactivity, we detected significantly increased levels of TREM2 in AD FC in terms of intensity of fluorescence (Figure 1E) and number of TREM2^{+} cells over the total number of cells around plaques (Figure 1F). Interestingly, significantly higher levels of TREM2 were found also in NDAN patients versus AD. Both images (Figure 1D) and quantitative analyses (Figure 1E,F) showed a significant higher number of TREM2^{+} cells detected around Aβ plaques in NDAN

FIGURE 1 Expression and distribution of IBA1 and TREM2 in relation to β-amyloid (Aβ) plaques in age-matched, Alzheimer's disease (AD), and Nondemented with AD neuropathology (NDAN) subjects. (A–C) Double immunofluorescence (IF) showing higher distribution of microglial cells (red) around Aβ plaques (green) in NDAN individuals as compared to AD and controls. White arrowheads indicate microglia attacking amyloid deposits in AD and NDAN. Scale bar 30 μm. Quantitative analyses of images show significantly increased IntDen levels of IBA1 and number of IBA^{+} cells in NDAN versus AD and controls. Statistical analyses were made using one-way analysis of variance (ANOVA), followed by Tukey's multiple-comparisons test. Values are expressed as the mean ± SD. (B) Ctrl versus. AD ** $p = 0.0074$; AD versus NDAN * $p = 0.0369$; ctrl versus. NDAN **** $p < 0.0001$. (C) Ctrl versus AD **** $p < 0.0001$; AD versus NDAN *** $p = 0.0002$; ctrl versus NDAN **** $p < 0.0001$. (D–F) double IF staining showing higher distribution of TREM2 (red) around Aβ plaques (green) in NDAN individuals as compared to AD and controls subjects. Images and quantitative analyses show increased number of TREM2^{+} cells surrounding plaques in NDAN versus. AD. Scale bar 30 μm. Statistical analyses were made using one-way ANOVA, following Tukey's multiple-comparisons test. Values are expressed as the mean ± SD. (E) Ctrl versus AD ** $p = 0.0016$; AD versus NDAN ** $p = 0.0011$; ctrl versus NDAN **** $p < 0.0001$. (F) Ctrl versus AD * $p = 0.0232$; AD versus NDAN ** $p = 0.0078$; ctrl versus NDAN **** $p < 0.0001$. (G,H) triple IF and quantitative analyses showing higher number of TREM2 $^{+}$ (magenta) IBA^{+} (green) cells over the total number of microglia in NDAN than in AD subjects around Aβ plaques. Scale bar 30 μm. Statistical analyses were made using t-test. Values are expressed as the mean ± SD. AD versus NDAN *** $p = 0.0002$

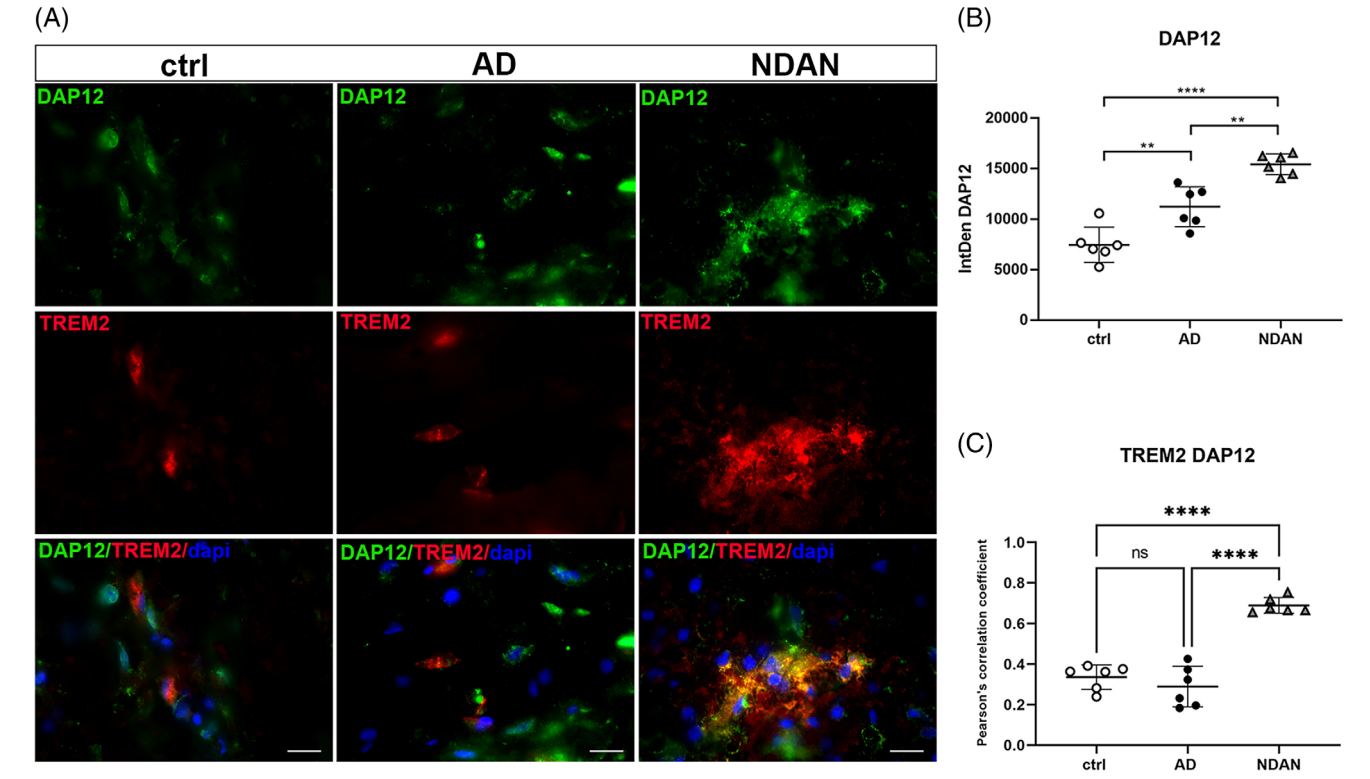

FIGURE 3 Expression and distribution of DAP12 and colocalization with TREM2 in aged-matched, Alzheimer's disease (AD), and Nondemented with AD neuropathology (NDAN) subjects. (A,B) Immunofluorescence (IF) staining and quantitative analysis showing increased distribution of DAP12 (green) in AD and NDAN individuals as compared to controls subjects. (A–C) Double staining with TREM2 (red) and Pearson's correlation coefficient analysis showing increased levels of colocalization in NDAN versus AD and control subjects. Statistical analyses were made using one-way analysis of variance, followed by Tukey's multiple-comparisons test. Values are expressed as the mean ± SD. B) Ctrl versus AD ** $p = 0.0031$; AD versus NDAN ** $p = 0.0012$; $p < 0.01$; ctrl versus NDAN **** $p < 0.0001$. C) Ctrl versus AD $p = 0.5078$; AD versus NDAN **** $p < 0.0001$; ctrl versus NDAN **** $p < 0.0001$

individuals (white arrowheads) as compared to AD patients and normally aged individuals. Furthermore, when we performed a triple staining of TREM2 in combination with IBA1 and Aβ (Figure 1G), surprisingly we found a significant increased number of microglial cells around Aβ plaques expressing TREM2 in NDAN frontal cortex as compared to AD (Figure 1H). Considering the fundamental role of TREM2 in conferring the phagocytic profile to microglia [23], a higher commitment of NDAN microglia toward the phagocytic pathway might be suggested.

To shed light onto the overall expression and distribution of TREM2 in AD and NDAN individuals, we investigated the distribution of TREM2 not only in the proximity of plaques, but also in areas of frontal cortex without amyloid deposits, using IF and western blotting (Figure 2). Interestingly, the extensive analyses of the immunoreacted sections revealed higher levels of TREM2 in NDAN individuals, regardless of the presence of Aβ plaques as compared to controls and AD patients. Furthermore, the latter show significantly lower levels of TREM2 when compared to aged-matched controls and NDAN (Figure 2 A, B). These findings were confirmed by WB analyses performed on frontal cortex total lysates (Figure 2C).

2.2 | NDAN individuals display increased levels of phagocytic microglia

The complex formed by TREM2 and its protein adaptor DAP12 is required for the activation of the microglial phagocytic pathway [23]. To investigate the trend of NDAN microglia toward the phagocytic phenotype, we evaluated the expression and distribution of DAP12 in relation to TREM2, performing double IF in post-mortem FC of controls, AD, and NDAN (Figure 3A). When we analyzed the overall distribution of DAP12 per se, we found significantly increased levels of DAP12 in NDAN as compared to AD and controls (Figure 3B). Also, the evaluation of the colocalization between TREM2 and DAP12 using the Pearson's correlation coefficient analysis showed significant colocalization levels between TREM2 and DAP12 in NDAN versus AD, whereas no significant differences were detected between normally aged individuals and AD patients (Figure 3C).

2.3 | NDAN are hallmarked by hyperactive microglia around Aβ plaques

To understand the activation state of microglia around Aβ plaques we performed a triple staining of Aβ in

combination with IBA1 and CD68 (Figure 4A–C), the latter considered as a microglial lysosomal and activated microglia marker [28]. Significantly increased levels of CD68 were detected in the proximity of Aβ plaques in NDAN individuals versus AD (as indicated by the white arrowhead) (Figure 4A) in terms of integrated density

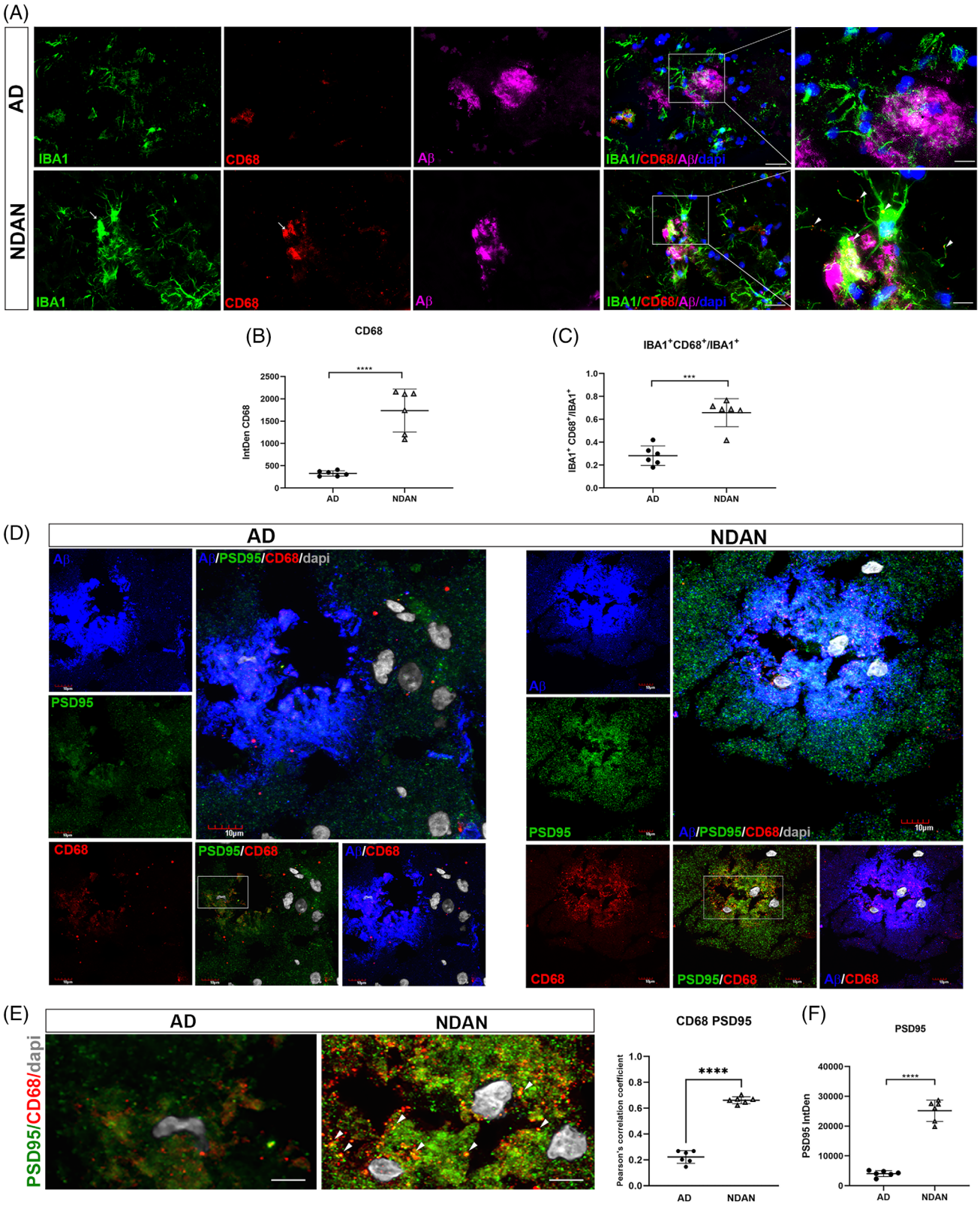

FIGURE 4 Legend on next page.

(Figure 4B) and number of $CD68^+$ $IBA1^+$ cells over the total number of $IBA1^+$ cells (Figure 4C). The microglial cells surrounding Aβ plaques, showed in higher magnification images, displayed the typical bushy/amoeboid phagocytic shape, suggesting a prominent activation of phagocytic microglial population in the nondemented AD versus demented AD individuals.

To test the phagocytic efficiency of this highly active microglia in the removal of damaged synapses, we marked microglial lysosomes with CD68, and we looked for its colocalization with PSD95 (a postsynaptic marker), around Aβ plaques. Confocal images (Figure 4D) further confirmed the presence of hyperactive microglia around plaques in NDAN as supported by the increased levels of CD68. Moreover, significantly increased levels of PSD95 were detected in NDAN individuals versus AD and quantitatively analyzed around Aβ plaques (Figure 4F). Importantly, we found colocalization between PSD95 and CD68 in NDAN (but not in AD) clearly indicating the engulfment of synapses (green) by the microglial lysosomes (red), as shown in Figures 4E in higher magnification images (white arrowheads). The Pearson's correlation coefficient analysis confirmed higher colocalizations levels between PSD95 and CD68 in NDAN as compared to that of AD subjects.

2.4 | Healthy synapses surround Aβ plaques of NDAN individuals

The presence of highly activated microglia around plaques in NDAN individuals prompted us to investigate the preservation of synaptic integrity. We performed double IF of Aβ in combination with either MAP2 or βIII Tubulin as dendritic and axonal markers, respectively (Figure 5A,B). The images and the quantitative analyses showed significantly lower levels of MAP2 in AD as compared to controls, while NDAN individuals were found to exhibit significantly increased levels of MAP2 as compared to both control and AD around plaques (Figure 5A). Similarly, AD patients displayed a significant decrease of βIII tubulin levels in proximity of plaques, while NDAN showed preserved levels of this axonal marker, comparable to control individuals (Figure 5B).

It has been recently reported that the formation of synaptophysin bodies along the axons represents a reliable axonal damage marker. Particularly medium-sized synaptophysin bodies (2–7.5 μm diameter), and large-sized bodies (8–15 μm) are associated with axonal transport disturbances [29]. We performed double staining for Aβ and synaptophysin in AD and NDAN and we analyzed approximately 25 synaptophysin bodies per subject around plaques (5 bodies/section) (Figure 5C). Images visibly demonstrated the presence of a lower number of medium/large synaptophysin bodies in NDAN than AD, where instead numerous large bodies were recognizable. Indeed, quantitative analysis of the size of synaptophysin bodies demonstrated a significantly higher percentage of medium/large synaptophysin bodies in AD as compared to NDAN, where instead the majority of bodies detected were small in size (0–2 μm) thus associated with physiological conditions. The highest presence of small synaptophysin bodies in NDAN versus AD were also confirmed when the distribution of synaptophysin bodies were analyzed individually (Figure S2). This data further confirmed the state of preservation of axonal structure in the NDAN subjects despite the activity of toxic Aβ.

2.5 | NDAN microglia efficiently recognize ePS on damaged synapses

In view of the important role played by ePS in mediating the phagocytic activity of microglia through the binding with TREM2, we indirectly evaluated the levels of ePS in FC of normally aged subjects, AD and NDAN individuals through flow cytometry ANXV assay and super resolution microscopy (Figure 6). Firstly, as fully described in the method section, we measured the levels of ePS by quantifying the percentage of intact synaptosomes positive for ANXV. Surprisingly, we found significantly higher levels of ePS in NDAN individuals as compared to AD, and no significant differences between age-matched subjects and NDAN, perhaps indicative of a higher capability to expose phosphatidylserine by NDAN

FIGURE 4 Expression and distribution of phagocytic microglia and engulfed synapses in relation to β-amyloid (Aβ) plaques in Alzheimer's disease (AD) and Nondemented with AD neuropathology (NDAN) individuals. (A) Triple immunofluorescence (IF) of IBA1 (green) in combination with CD68 (red) and Aβ (magenta) showing significantly increased levels of activated microglia in NDAN individuals. Scale bar 30 μm. Higher magnification images showing highly phagocytic macroglia surrounding NDAN plaques. Microglial lysosomes are indicated with white arrowheads. Scale bar 10 μm. (B) Quantitative analyses of total CD68 levels, (C) and the counting of microglial cells positive to CD68 confirming the presence of highly phagocytic microglia in NDAN versus AD around plaques. Statistical analyses were made using *t*-test. Values are expressed as the mean ± SD. (B) **** $p < 0.0001$; (C) *** $p = 0.0001$. (D) Confocal images of AD and NDAN FC confirming higher immunoreactivity levels of CD68 (red) in NDAN versus AD indicating the presence of activated microglia in the proximity of Aβ plaques (blue). (E) Higher magnification images and Pearson's correlation coefficient analysis demonstrate significantly higher colocalization levels between CD68 and PSD95 in NDAN as compared to AD FC. The white arrows indicate the engulfment of synapses (green) by the microglial lysosomes (red) in NDAN. Statistical analyses were made using *t*-test. Values are expressed as the mean ± SD. **** $p < 0.0001$. Scale bar 10 μm. (F) NDAN microglia phagocytic activity in removing damaged synapses is supported by the significantly higher levels of PSD95 in NDAN versus AD near Aβ plaques. Statistical analyses were made using *t*-test. Values are expressed as the mean ± SD. **** $p < 0.0001$

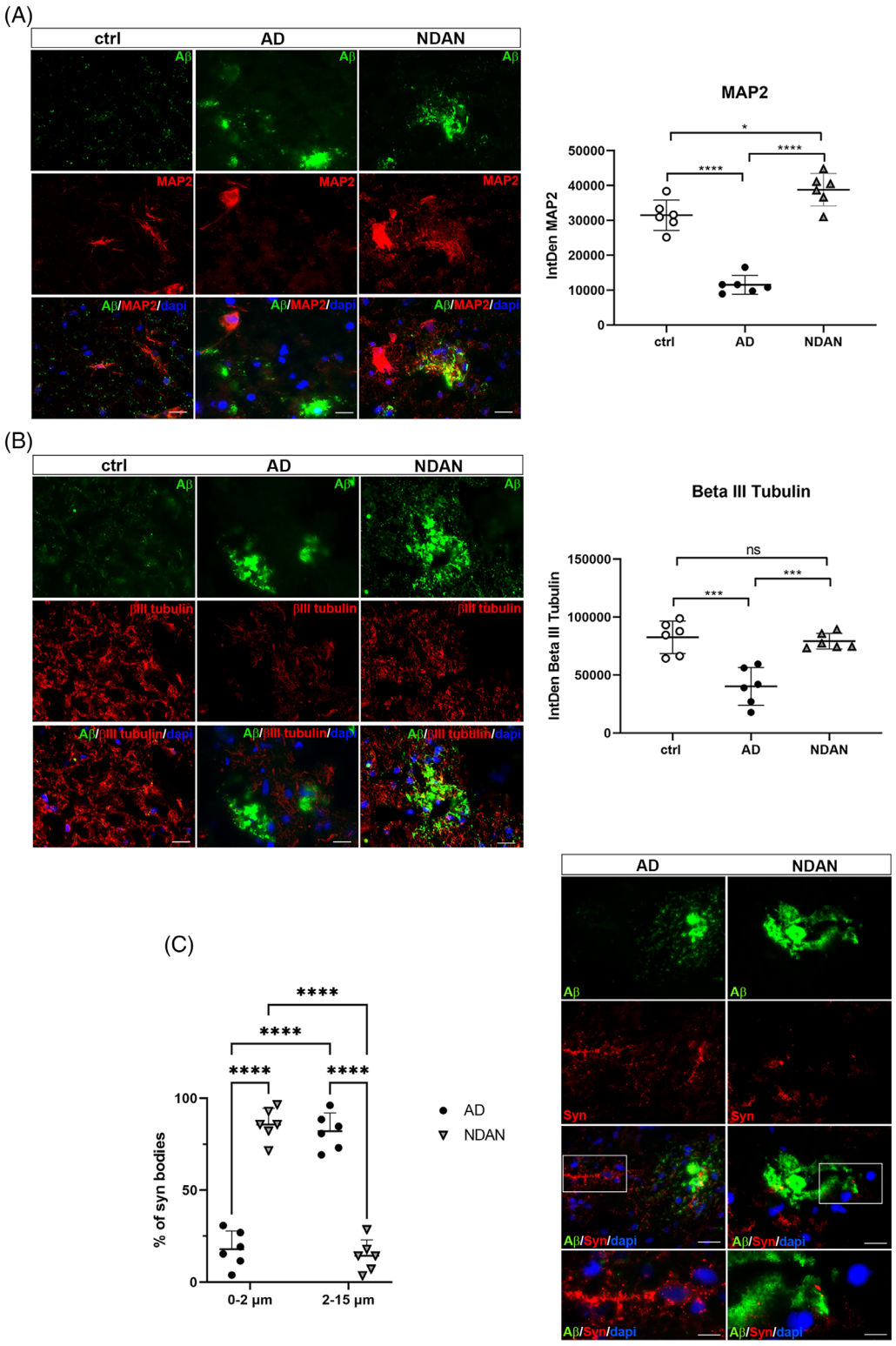

FIGURE 5 Expression and distribution of axonal and dendritic markers in aged-matched, Alzheimer's disease (AD), and Nondemented with AD neuropathology (NDAN) subjects. (A) Double immunofluorescence (IF) staining and quantitative analysis showing higher distribution of MAP2 (red) around β-amyloid (Aβ) plaques (green) in NDAN individuals as compared to AD and control subjects. Scale bar 30 µm. (B) Double IF staining and quantitative analysis demonstrating higher distribution of βIII tubulin (red) around Aβ plaques (green) in NDAN individuals as compared to AD. (C) Representative images of double staining of Syn (red) in combination with Aβ (green) (scale bar 30 µm) and higher magnification micrographs (scale bar 10 µm). Quantitative analyses of the size of syn bodies confirmed NDAN axonal integrity. Statistical analyses were made using one-way analysis of variance, followed by Tukey's multiple-comparisons test. Values are expressed as the mean ± SD. (A) Ctrl versus AD **** $p < 0.0001$; AD versus NDAN **** $p < 0.0001$; ctrl versus NDAN * $p < 0.0168$. (B) Ctrl versus AD *** $p = 0.0001$; AD versus NDAN ***$p = 0.0003$; ctrl versus NDAN $p = 0.8983$. C) Statistical analyses were made using *t*-test. Values are expressed as the mean ± SD. **** $p < 0.0001$

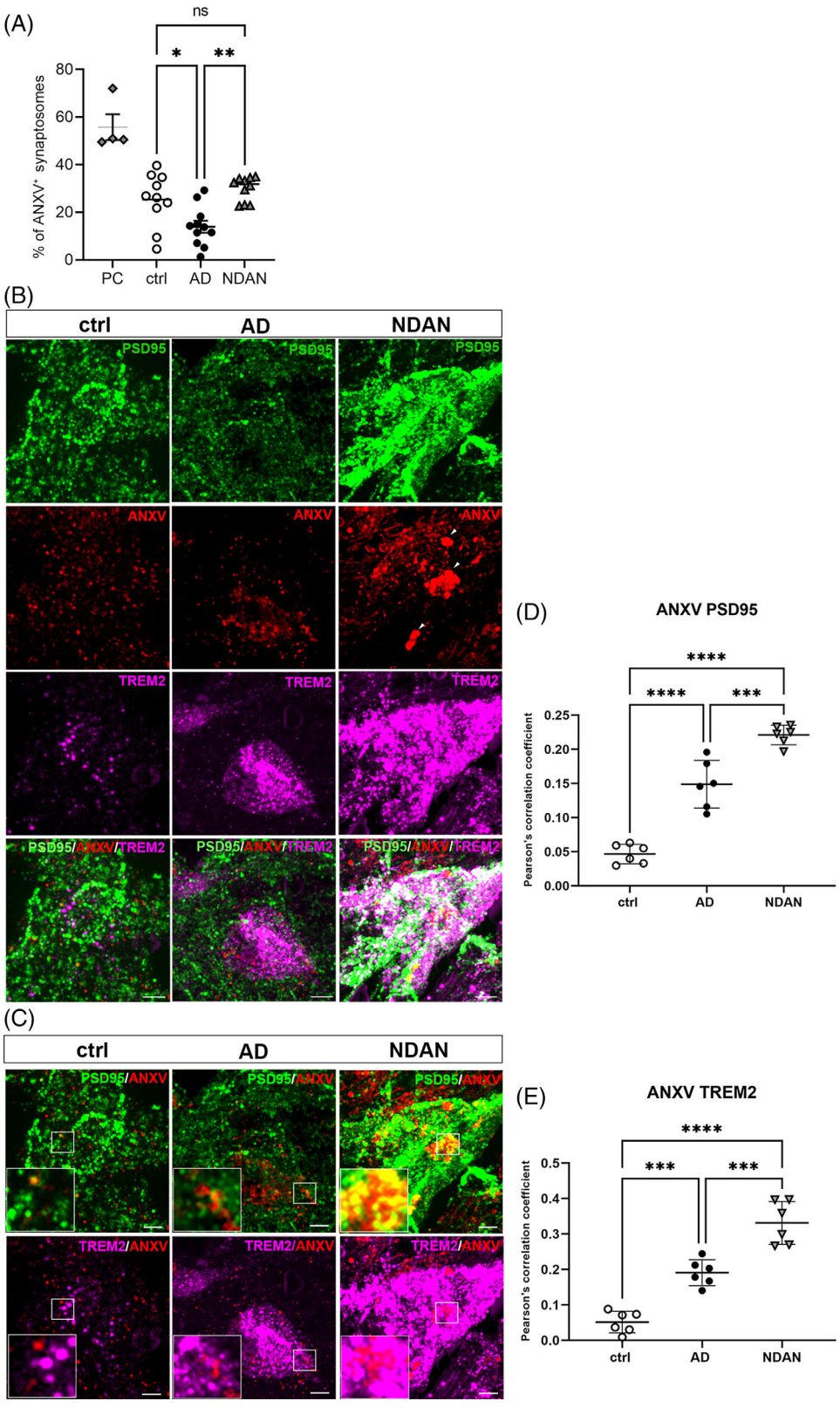

FIGURE 6 Evaluation of exposed phosphatidylserine in control, Alzheimer's disease (AD), and Nondemented with AD neuropathology (NDAN) frontal cortices (FC). (A) Flowcytometry ANXV assay of human synaptosomes isolated from FC of aged-matched, AD and NDAN individuals showing significantly increased percentage of intact synaptosomes positive for ANXV in NDAN as compared to AD subjects. Statistical analyses were made using one-way ANOVA, following Tukey's multiple-comparisons test. Values are expressed as the mean ± SD. Ctrl versus AD * $p = 0.0279$; AD versus NDAN ** $p = 0.0014$; ctrl versus NDAN $p = 06733$. PC, positive control. (B,C) Representative images of triple immunofluorescence staining of PSD95 (green) in combination with ANXV (red) and TREM2 (magenta) of age-matched, AD, and NDAN subjects, showing increased levels of ANXV, PSD95 and TREM2 and the colocalization (white) among these three markers in NDAN individuals. Scale bar 5 μm. (D,E) Pearson's correlation coefficient analyses of colocalization show increased levels of colocalization between ANXV and either PSD95 or TREM2 in NDAN as compared to AD and controls. Statistical analyses were made using one-way analysis of variance, following Tukey's multiple-comparisons test. Values are expressed as the mean ± SD. (D) Ctrl versus AD **** $p < 0.0001$; AD versus NDAN *** $p = 0.0002$; ctrl versus NDAN **** $p < 0.0001$. (E) Ctrl versus AD *** $p = 0.0002$; AD versus NDAN *** $p = 0.0002$; ctrl versus NDAN **** $p < 0.0001$

damaged synapses (Figure 6A). As mentioned before, the neuronal ePS eat-me signal on damaged synapses is recognized by microglia through a phagocytic TREM2-mediated mechanism [12]. Therefore, to elucidate the hypothesized efficient engulfment of damaged synapses in NDAN individuals, we performed a triple staining of PSD95 and TREM2 in combination with ANXV, the latter to label ePS. Super resolution 320× magnification images qualitatively demonstrated increased colocalization (white) among PSD95 (green), ANXV (red) and

TREM2 (magenta) in NDAN FC as compared to AD and age-matched subjects (Figure 6B,C), proving the identification of damaged synapses by microglial TREM2. Furthermore, NDAN individuals showed a clustered staining for ANXV as shown in Figure 6C and indicated by the arrows. The Pearson's correlation coefficient analyses used to quantify the colocalization shows significantly higher levels of colocalization between ANXV and either PSD95 or TREM2 in NDAN individuals as compared to AD and control subjects (Figure 6D,E).

3 | DISCUSSION

The aim of this work was to investigate the cellular mechanisms underlying the activity of microglia against Aβ accumulation and the response elicited by Aβ-mediated toxicity in both AD patients and NDAN individuals. Specifically, our goal was to shed light onto possible mechanisms involved in cognitive resilience, peculiar of NDAN subjects. In the last decades, the idea that proliferation and activation of microglia in the brain, concentrated around plaques, and the view of microglia and neuroinflammation as prominent features in AD, have received growing attention [27]. It is well accepted that around Aβ plaques, high concentrations of soluble Aβ are released, causing damage to synapses close to the plaques themselves; also, the dystrophic synapses are engulfed and removed by microglia that are promptly recruited on the site of damage. Depending on the efficiency of microglia, synaptic dysfunctions spread along the axons or are limited to the proximity of the plaques [10]. Based on this evidence, we decided to investigate the efficiency of microglial activity as one of the mechanisms operated by NDAN to preserve synaptic integrity. To accomplish our aim, we carried out a comprehensive study of human post-mortem FC that included age-matched controls, demented and nondemented individuals with AD pathology, using IF and flow cytometry techniques. We addressed the interaction between microglia and Aβ plaques detecting the expression and distribution of specific microglial markers in relation to Aβ plaques. Firstly, we analyzed the expression of IBA1, commonly used as a marker of microglia, regardless of their activation state. The higher expression of IBA1 and the increased number of IBA^+ cells around plaques in AD patients suggest an Aβ-mediated microglial response in the vicinity of plaques. This is consistent with the widely accepted concept whereby homeostatic microglia respond to Aβ accumulation and neurodegenerative lesions, by progressively acquiring a unique transcriptional and functional signature, and evolving into disease-associated microglia (DAM) [17, 30, 31]. Moreover, it has been extensively described that DAM is able to slow the progression of neurodegeneration in certain mouse models; however, inappropriate activation of microglia could exacerbate neurodegenerative disease in other models and in human AD [32, 33]. With this in mind, data concerning NDAN patients are particularly enlightening, since the significantly augmented levels of IBA1 around plaques versus AD, could represent an example of DAM exerting neuroprotective effects. We can speculate that NDAN may be characterized by a more efficient microglial activation, responsible for a more efficient removal of debris around the synapses, thus avoiding further spreading of damage. This vision could be strengthened by the results we obtained by IF, where significantly increased levels of CD68, marker of microglial lysosomes that identifies activated and phagocytic microglia, were found in NDAN as compared to AD. These findings suggest that NDAN individuals are hallmarked by highly hyperactive microglia, consistently with the hyper-ramified and bushy shape of microglial cells we detected surrounding and attacking plaques. It is worth emphasizing that microglia require TREM2 for the full acquisition of a DAM profile [17], in view of its ability to bind Aβ [18], hence representing the bridge between microglia and Aβ. Furthermore, as the concentration of Aβ increases, TREM2 expression increases too, thus causing morphological change of microglia and leading to activation of signal transduction pathways regulating the removal of damaged synapses [10]. This scenario is well represented in both AD and NDAN patients in which we observed a higher number of $TREM2^+$ cells versus control subjects around and inside the plaques, where Aβ oligomers are particularly abundant. However, the significant overexpression of TREM2 and CD68 in NDAN as compared to AD, could be causative of an enhanced microglia efficiency in the engulfment of dystrophic neurites, thus decreasing the release of Aβ from damaged boutons and limiting the spread of further damage to nearby neurites and therefore synaptic loss. This is consistent with evidence in literature describing the increased TREM2 levels as protective against Aβ toxicity in different mouse models of AD ([34–37]). The neuroprotective activity of TREM2 in NDAN is also supported by its augmented levels regardless of the presence of plaques as compared to controls and AD patients. The data suggest that, in some way, TREM2 could be constitutively expressed at higher levels in NDAN individuals, thus exerting an anti-inflammatory and neuroprotective action, and increasing the surveillance activity of microglia. In this regard, it is worth noticing that TREM2 signaling has anti-inflammatory consequences and has been shown to antagonize Toll-like receptor (TLR-4) mediated inflammation by modulating the JNK and suppressing NFκB signaling pathways [23, 38]. It is conceivable that this higher expression of TREM2 represents a way for NDAN individuals to preserve synaptic activity and resist the harmful effect of Aβ and therefore dementia.

The highest capability of NDAN to engulf damaged synapses might be related to their enhanced competence in activating an efficient phagocytic microglial pathway. Notably, the activation of TREM2-dependent phagocytic

pathway requires the activation of the SYK/PI3K/AKT/PLCγ pathways [23], which occurs after the dimerization of TREM2 with its adaptor protein DAP12 [20–22]. Our findings showing increased levels of colocalization between TREM2 and DAP12 might underlie the efficient triggering of phagocytic mechanism that is responsible of debris and injured synapses removal. The adequate phagocytic activity may provide protection from the spreading of the damage, which is restrained around Aβ plaques, saving NDAN synapses from disruption. This idea is well consistent with the results we obtained studying the axonal and dendritic structure around Aβ plaques, where NDAN individuals were found to display very well-preserved structure, mostly compared to aged matched nondemented individuals. Furthermore, AD patients showed disrupted synapses, as indicated by the significantly decreased levels of axonal and dendritic markers. Consistent with the preservation of synapses in NDAN individuals, data regarding the expression of PSD95 around plaques in AD and NDAN are especially remarkable. The significantly increased levels of PSD95 found around plaques in NDAN, as compared to AD patients, might indicate a higher efficiency of the phagocytic pathway underlying a well-competent TREM2-mediated repair mechanism and dynamic synaptic pruning. Furthermore, in NDAN, but not in AD, we found evidence of the engulfment of damaged synapses, through the visualization of PSD95 inside the microglial lysosomes labeled with CD68, and thus proved the fundamental and well-known role of microglia in synaptic pruning and remodeling during physiological and pathological conditions [12, 38, 39].

It has been recently described that ePS plays an extremely important role in the microglial-mediated elimination of damaged synapses; also, numerous phagocytic receptors that are involved in the recognition of ePS are expressed by microglia and astrocytes, including TREM2 [19]. It is worth noting that TREM2 has also been found to be required in the physiological synapse elimination and normal brain connectivity [39]. In view of this evidence, we developed a protocol to evaluate the levels of ePS on human synaptosomes from age-matched subjects, AD, and NDAN individuals. The significantly increased levels of ANXV found in NDAN individuals compared to AD FC could indicate a higher capability of the formers to expose damaged synapses to microglia with respect to AD subjects. Furthermore, super resolution images confirmed our hypothesis of an efficient recognition of damaged synapses by microglial TREM2, as supported by the high degree of colocalization detected among the synaptic marker PSD95, the damage marker ANXV and the microglial receptor TREM2.

The present work brings new evidence on the role of homeostatic and phagocytic microglia in AD pathology and the mechanisms underlying the elicited neuroinflammatory response. In this work we described for the first time that an efficient activation of TREM2-mediated phagocytosis might underlie synaptic resilience in NDAN individuals. The hypothesized competent engulfment of injured synaptic boutons from NDAN microglia in the proximity of Aβ plaques could represent an aspect of a much greater scenario where NDAN individuals trigger a repair mechanism, mediated by microglia, to maintain synaptic integrity. Indeed, it is not unreasonable to speculate that the efficient flipping of PS occurring at NDAN synapses is paired with the competent activation of the TREM2-mediated phagocytosis in Aβ plaques-associated microglia: the combination of these two processes leads to the removal of damaged synapses, thus halting the spreading of the damage. We here describe for the first time the occurrence of a highly efficient mechanism of synaptic pruning associated to Aβ pathology. Overall, our work demonstrates that NDAN individuals may be hallmarked by a new type of DAM, specifically localized near Aβ plaques, characterized by increased phagocytic efficiency that is ultimately associated with synaptic resilience and preservation of cognitive integrity despite the presence of substantial AD neuropathology.

4 | EXPERIMENTAL PROCEDURES

4.1 | Human subjects and autopsy of brain tissues

Post-mortem brain tissues were obtained from the Oregon Brain Bank at Oregon Health and Science University (OHSU), in Portland, OR (USA). Donor subjects of either sex were enrolled and clinically evaluated in studies at the NIH-sponsored Layton Aging and AD Center (ADC) at OHSU, in accordance with protocols that were approved by the OHSU Institutional Review Board (IRB). Informed consent was obtained from all participants prior to their enrolment in the studies at the ADC. Subjects were participants in brain aging studies at the ADC and received annual neurological and neuropsychological evaluations, with a clinical dementia rating (CDR) assigned by an experienced clinician. A neuropathological assessment was performed at autopsy, and in compliance with IRB-approved protocols. A neuropathologist scored autopsy brain tissue for Aβ plaques and NFTs, according to standardized CERAD criteria and Braak staging [40]. Participants were classified as AD when possessing a National Institute for Neurological and Communicative Disorders and Stroke-Alzheimer's Disease and Related Disorder Association diagnostic criteria for clinical AD (CDR) including a mini-mental state exam (MMSE) [41] score below 10. Control participants performed normally in cognitive examinations (MMSE of 29–30). NDAN cases displayed little to no cognitive impairment (MMSE 27 or greater), though at autopsy it was revealed presence of amyloid plaques and NFTs comparable to fully symptomatic AD (Table 1). Donor subject samples were de-identified by ADC prior to being

TABLE 1 Clinical data of the subjects used in the study

Case number	Diagnosis	Age	Sex	Braak stage	MMSE	PMI (h)
767	ctrl	86	F	2	29	8
1525	ctrl	89	F	1	29	3
1731	ctrl	74	F	2	29	7.5
2467	ctrl	99	F	3	28	4.5
2953	ctrl	100	F	2	20	2.5
2553	ctrl	100	M	2	28	4
785	ctrl	83	M	1	29	<14
986	ctrl	83	M	1	N/A	2
1013	ctrl	89	M	1	29	6
2682	ctrl	90	F	2	29	9
2755	ctrl	95	F	2	29	18
3200	ctrl	90	M	2	20	4.5
1538	AD	84	M	5	26	5.5
2472	AD	96	F	6	27	5
2312	AD	87	F	6	N/A	2.5
1774	AD	>89	M	6	22	3.25
1776	AD	>89	F	6	26	6.25
2543	AD	95	M	6	21	5
2315	AD	95	M	4	N/A	4
2317	AD	88	M	6	N/A	4
2318	AD	74	F	6	N/A	2
1791	AD	103	M	4	N/A	10
1969	AD	67	F	6	N/A	13
2010	AD	87	F	3	N/A	6
2201	AD	86	M	6	N/A	16
2221	AD	93	F	6	N/A	15
2272	AD	90	F	6	20	5
697	NDAN	>89	M	5	29	5
1016	NDAN	>89	F	6	26	8
1179	NDAN	>89	F	4	27	2.5
1686	NDAN	87	F	4	29	2.5
2376	NDAN	93	M	4	26	4
2980	NDAN	98	F	4	27	4
1578	NDAN	89	M	5	27	15.5
2474	NDAN	90	F	4	28	8
3178	NDAN	93	M	3	29	10
1284	NDAN	91	M	5	27	5
2322	NDAN	89	F	4	29	14
2491	NDAN	82	M	4	28	8

Notes: Average PMI, Ctrl (6.3 h), Alzheimer's disease (AD) (6.8 h), Nondemented with AD neuropathology (NDAN) (7.4 h); Braak stage, A measure of the number and location of tau tangles and β-amyloid plaques in the brain; MMSE, Mini mental state examination (administered within the last year); PMI, Post-mortem interval.

provided to University of Texas Medical Branch (UTMB), so that no approval was required from the UTMB IRB under CFR §46.101(a) [1]. The cases used in this study are described in Table 1.

To ensure that the variations in post-mortem interval (PMI) did not affect the measurements, we performed a correlation analysis between PMI values and results obtained in the various assays presented here using a Pearson's correlation test. No correlation was found between PMI values and any of the elements/antigens studied here (Figure S3), and therefore observed differences could not be attributed to differences in nonspecific post-mortem tissue degradation. However, even though the results shown in Figure S3 reassure on the data

regarding the different antigens studied here, it is important to appreciate that brains with PMI >10 h might not necessarily fully reflect freshly obtained brain tissue.

4.2 | Tissue processing and IF

Fresh frozen cortical tissue blocks (n = 6/group) were removed from storage at −80°C, equilibrated at −20°C, embedded in O.C.T. compound (catalog# 4583, Tissue-Tek) and sectioned at 12 μm onto Superfrost/Plus slides (catalog# 12-550-15, Fisherbrand, ThermoFisher Scientific). Prepared slides were stored at −80°C until use. For the ANXV staining frozen sections were incubated with R-phycoerythrin conjugated ANXV (1:50) (catalog# A35111 Thermo Fisher) diluted in ANXV binding buffer (10 mM HEPES, 140 mM NaCl, and 2.5 mM $CaCl_2$, pH 7.4) for 15′ at room temperature (RT) and rinsed in phosphate-buffered saline solution (PBS) prior fixation. For regular immunostainings, slides were fixed in 4% paraformaldehyde in 0.1 M PBS, pH 7.4 for 30 min at RT. Nonspecific binding sites were blocked with 5% bovine serum albumin (catalog# A4503-100G, Sigma-Aldrich Inc.)/10% normal goat serum (NGS, catalog# S26-100 ml Sigma-Aldrich) and sections were permeabilized with 0.5% Triton X-100/0.05% Tween-20 for 1 h at RT. Slides were incubated with the following primary antibodies, diluted in PBS containing 1.5% NGS/overnight at 4°C: mouse anti-Aβ 4G8 clone (1:100, catalog# 800708, RRID: AB_2734547, BioLegend); rabbit anti-Aβ (1:200 catalog# ab201060, RRID:AB_2818982, Abcam – Cambridge Science Park) rabbit anti-IBA1 (1:200, catalog#19741, FUJIFILM Wako, RRID:AB_839504); rabbit anti-TREM2 (1:500, catalog# ab209814, Abcam); rat anti-TREM2 (1:200, catalog# ab86491, RRID:AB_1925525, Abcam); rabbit anti-DAP12 (1:200 catalog# ab124834, RRID:AB_10971363, Abcam); rat anti-CD68 (1:200, catalog# ab53444, RRID:AB_869007, Abcam); mouse-anti PSD95 (1:200, catalog #ab13552, RRID:AB_300453, Abcam); chicken anti-MAP2 (1:500, catalog #MAP, RRID:AB_2313549, Aves Labs); rabbit anti βIII tubulin (1:200, catalog# ab18207 Abcam, RRID:AB_444319).

Slides were washed in PBS before incubation with the appropriate Alexa-conjugated secondary antibodies (goat anti-rabbit Alexa Fluor 488, 1:400, Cat# A-11008, RRID: AB_143165; goat anti-mouse Alexa Fluor 594, 1:400 Cat# A-11032, RRID:AB_2534091; goat anti-mouse Alexa Fluor 488, 1:400 Cat# A-10680, RRID:AB_2534062; goat anti-chicken Alexa Fluor 594, 1:400, Cat# A-11042, RRID:AB_2534099; ThermoFisher Scientific) in PBS containing 1.5% NGS/0.25% Triton X-100 for 1 h at RT. Finally, slides were washed in PBS, treated with 0.3% Sudan Black B prepared in 70% EtOH for 10 min to block lipofuscin autofluorescence, washed again with deionized water, and coverslipped using Fluoromount-G containing 4′,6-diamidino-2-phenylindole (DAPI) (Cat# 0100-20, SouthernBiotech) and sealed.

4.3 | Quantitative microscopy

All immunoreacted sections were acquired with either a Keyence BZ-X800 (Keyence Corporation) microscope or IX83 Confocal microscope (Olympus Corporation), by using immersion oil 60X and 100× objectives. Super resolution images were taken with the Olympus IXplore SpinSR Super Resolution Microscope System (Olympus Corporation). For all analyses each subject was analyzed as follows. Four sections were analyzed for each individual and at least three images per section were taken at 1920 × 1440 pixel resolution, with z-step size of 2 at 12 μm thickness. For the feasibility of the quantification, all layers from a single image stack were projected on a single slice (stack/Z projection). Quantitative analyses were performed using ImageJ software (https://imagej.nih.gov/ij, NIH). The analysis of each marker was made in relation to Aβ plaques and a plaque microenvironment of approximately 100 μm of diameter was considered as region of interest (see Figure S4). Plaques were selected for their similar size, location, and cortical area. We analyzed the intensity of fluorescence for each marker per area (Integrated Density, IntDen) when the overall distribution of a specific marker was studied, and the manual counting of positive cells for the specific marker in the plaque microenvironment, when the quantitative counting of cells was performed. The colocalization between two markers was evaluated and quantified using the Pearson's correlation coefficient. Representative images were composed in an Adobe Photoshop CC2020 format.

4.4 | Western blot analysis

25 mg frontal cortex tissue was homogenized in 1× RIPA buffer (#9806, Cell Signaling Technology Inc.) containing 1 mM PMSF, 1 × Halt™ Protease and Phosphatase Inhibitor Cocktail (ThermoScientific) on ice. Tissue lysate was centrifuged for 15 min at 15,000 × g, 4°C. Protein concentrations were measured using the Bio-Rad protein assay kit (Bio-Rad Laboratories, Inc.). Protein lysates (10 μg) were resolved by 4%–15% SDS-PAGE (Criterion™ TGX™, Bio-Rad Laboratories, Inc.), electrophoretically transferred to polyvinylidene difluoride membranes (Immobilon®-P, Millipore) subject to immunoblotting analysis. Primary antibodies were used as follows: rabbit anti-TREM2 (ab209814, Abcam, 1:1000), mouse anti-β-actin (1:10,000 A1978, Sigma-Aldrich, RRID:AB_476692). HRP-conjugated secondary antibodies were used anti-rabbit IgG (1:5000 catalog# 7074, RRID:AB_2099233, Cell signaling) and antimouse IgG (1:5000 #7076, RRID:AB_330924, Cell signaling) 1 h at RT. Signal detection was performed with Electrochemiluminescence Western Blotting Detection Reagents (Amersham Biosciences). Expression levels were evaluated by quantification of the relative density of each band normalized to that of the corresponding β-actin band density, using ImageJ (NIH).

4.5 | Synaptosomes isolation and flow cytometry analyses

Synaptosomes were isolated using a standardized method developed in our laboratory and routinely used to assess synaptic dysfunction in our studies [42, 43]. Briefly, fresh frozen cortical brain tissues from age-matched, AD, and NDAN subjects ($n = 10$/group) were homogenized in Syn-PER synaptic protein extraction reagent (catalog# 87793, ThermoFisher Scientific) containing 1X Protease Inhibitor Cocktail (Sigma-Aldrich) and Halt Phosphatase Inhibitor Cocktail (Life Technologies, Inc). The total homogenate was centrifuged at 1200 × g for 10 min at 4 °C and the supernatant was collected and centrifuged further at 15,000 × g for 20 min at 4 °C. Pellet containing synaptosomes was resuspended in HEPES-buffered Krebs-like (HBK) buffer and 0.5% of F-68 nonionic surfactant (cat# 24040-032, ThermoFisher Scientific) was added to prevent synaptosome aggregation as previously described [44].

The quality and concentration of the isolated synaptosomes were assessed by electron microscopy and flow cytometry (Figure S5). Briefly, for transmission electron microscopy (Figure S5A), pellets of synaptosomes were fixed in a mixture of 2.5% formaldehyde and 0.1% glutaraldehyde in 0.05 M cacodylate buffer. After fixation, pellets were washed with 0.1 M cacodylate buffer and postfixed in 1% OsO4 in 0.1 M of cacodylate buffer, en bloc stained with 2% aqueous uranyl acetate in 0.1 M maleate buffer and gradually dehydrated in ethanol. Pellets were then infiltrated with graded mixtures of propylene oxide and Epon 812 (TAAB), and finally embedded in the same resin, and polimerized at 60°C for 3 days. Ultrathin sections were cut on Reichert-Leica Ultracut S ultramicrotome, stained with lead citrate, and examined in a Philips 201 or CM-100 electron microscope at 60 kV.

For flow cytometry quality control, synaptosomes were acquired by a Guava EasyCyte 8 flow cytometer (EMD Millipore) that contains a Class IIIb laser operating at 488 nm in continuous wave (CW) mode and a laser operating at 640 nm in CW mode. Forward scatter (FSC) and side scatter (SSC) properties determined the relative size and granularity of synaptosomes. FSC-SSC plots were generated and used to select particles matching the size of synaptosomes (0.75–5.0 μm) using calibrated beads (Spherotech Inc.) (Figure S5B). FSC, SSC, and fluorescent (yellow [580 ± 20 nm] and green [525 ± 30 nm]) signals were collected using log amplification. Identical FSC settings were used to acquire data on bead standards and samples. Small fragments and debris were excluded by establishing an FSC-H threshold (gain = 2). Settings for fluorescence amplification on green and yellow photomultiplier tube detectors were based on the emissions detected on size-based gated particles. ANXV and Calcein AM were detected by the yellow and green detectors, respectively (Figure S5B). A total of 5000 size-gated particles were collected for each sample, and analysis was performed using Incyte software (EMD Millipore).

4.6 | ePS evaluation by Annexin V assay

ePS was measured by quantify the PS binding protein ANXV conjugated with R-phycoerythrin in synaptosomes isolated from age-matched individuals, AD, and NDAN subjects. Briefly, 5×10^6 synaptosomes from each subject were suspended in 100 μl of ANXV-binding buffer (10 mM HEPES, 140 mM NaCl, and 2.5 mM $CaCl_2$, pH 7.4). Then the synaptosome suspension was incubated for 15 min at room temperature in the dark with 5 μl of a 1:50 diluted solution of ANXV R-phycoerythrin conjugated (catalog# A35111, Invitrogen) to label ePS and 5 μM of Calcein AM (catalog# 65–0853, Invitrogen) to label intact synaptosomes. After the incubation, 400 μl of ANXV-binding buffer was added to stop the reaction and the percentage of $ANXV^+$/Calcein-AM^+ synaptosomes was analyzed by flow cytometry. Synaptosomes in ANXV-binding buffer from control subjects incubated with 10 μM of Acrolein for 6 h at 37°C were used as positive control (PC) for ANXV binding as previously described [45].

4.7 | Statistical analyses

Statistical analyses were performed using Graphpad Prism 9.1.0 software. *t*-Test and one-way analysis of variance with Tukey's post hoc test were used to detect significant differences among groups. Data were then expressed as means ± SD and for all statistical analyses $p < 0.05$ was considered as statistically significant.

AUTHOR CONTRIBUTIONS

Anna Fracassi made substantial contribution to design of the study, performed morphological experiments, quantitative analyses and prepared draft of the manuscript; Michela Marcatti performed flow cytometry experiments; Batbayar Tumurbaatar performed western blotting experiments; Randall Woltjer provided human samples needed for the study, contributed to interpretation of data, and critically revised the manuscript. Sandra Moreno contributed to interpretation of data, and critically revised the manuscript. Giulio Taglialatela conceived, designed, and funded the study, and gave final approval of the version to be published. All authors read and approved the final manuscript.

ACKNOWLEDGMENTS

This work was supported by NIH/NIA grants R01AG069433 and R01AG060718 (to Giulio Taglialatela) and P30AG008017 (Randall Woltjer pathology core PI), and a grant from the Robert J. and Helen C. Kleberg Foundation to Giulio Taglialatela. The Grant of Excellence Departments, MIUR (Art. 1, L.232/2016), is gratefully acknowledged. We also wish to acknowledge Mr Simon Powell and Mr Shrinat Kadamangudi for technical support and Dr Salvatore Saieva for figures and text editing.

CONFLICT OF INTEREST

The authors declare no competing financial interests.

DATA AVAILABILITY STATEMENT

The data that support the findings of this study are available from the corresponding author upon reasonable request. The graphical abstract presented in this work has been generated using BioRender.

ORCID

Anna Fracassi https://orcid.org/0000-0001-9310-8982

REFERENCES

1. 2022 Alzheimer's disease facts and figures. Alzheimers Dement. 2022;18(4):700–89.
2. Jack CR Jr, Bennett DA, Blennow K, Carrillo MC, Dunn B, Haeberlein SB, et al. NIA-AA research framework: toward a biological definition of Alzheimer's disease. Alzheimers Dement. 2018;14(4):535–62.
3. Zolochevska O, Bjorklund N, Woltjer R, Wiktorowicz JE, Taglialatela G. Postsynaptic proteome of non-demented individuals with Alzheimer's disease neuropathology. J Alzheimers Dis. 2018;65(2):659–82.
4. Zolochevska O, Taglialatela G. Selected microRNAs increase synaptic resilience to the damaging binding of the Alzheimer's disease amyloid Beta oligomers. Mol Neurobiol. 2020;57(5):2232–43.
5. Bjorklund NL, Reese LC, Sadagoparamanujam VM, Ghirardi V, Woltjer RL, Taglialatela G. Absence of amyloid β oligomers at the postsynapse and regulated synaptic Zn2+ in cognitively intact aged individuals with Alzheimer's disease neuropathology. Mol Neurodegener. 2012;7:23.
6. Singh A, Allen D, Fracassi A, Tumurbaatar B, Natarajan C, Scaduto P, et al. Functional integrity of synapses in the central nervous system of cognitively intact individuals with high Alzheimer's disease neuropathology is associated with absence of synaptic tau oligomers. J Alzheimers Dis. 2020;78(4):1661–78.
7. Briley D, Ghirardi V, Woltjer R, Renck A, Zolochevska O, Taglialatela G, et al. Preserved neurogenesis in non-demented individuals with AD neuropathology. Sci Rep. 2016;6:27812.
8. Fracassi A, Marcatti M, Zolochevska O, Tabor N, Woltjer R, Moreno S, et al. Oxidative damage and antioxidant response in frontal cortex of demented and nondemented individuals with Alzheimer's neuropathology. J Neurosci. 2021;41(3):538–54.
9. Kashyap G, Bapat D, Das D, Gowaikar R, Amritkar RE, Rangarajan G, et al. Synapse loss and progress of Alzheimer's disease - a network model. Sci Rep. 2019;9(1):6555.
10. Edwards FA. A unifying hypothesis for Alzheimer's disease: from plaques to neurodegeneration. Trends Neurosci. 2019;42(5):310–22.
11. Sadleir KR, Kandalepas PC, Buggia-Prévot V, Nicholson DA, Thinakaran G, Vassar R. Presynaptic dystrophic neurites surrounding amyloid plaques are sites of microtubule disruption, BACE1 elevation, and increased Aβ generation in Alzheimer's disease. Acta Neuropathol. 2016;132(2):235–56.
12. Scott-Hewitt N, Perrucci F, Morini R, Erreni M, Mahoney M, Witkowska A, et al. Local externalization of phosphatidylserine mediates developmental synaptic pruning by microglia. EMBO J. 2020;39(16):e105380.
13. Gratuze M, Leyns CEG, Holtzman DM. New insights into the role of TREM2 in Alzheimer's disease. Mol Neurodegener. 2018;13(1):66.
14. Guerreiro R, Wojtas A, Bras J, Carrasquillo M, Rogaeva E, Majounie E, et al. TREM2 variants in Alzheimer's disease. N Engl J Med. 2013;368(2):117–27.
15. Jonsson T, Stefansson H, Steinberg S, Jonsdottir I, Jonsson PV, Snaedal J, et al. Variant of TREM2 associated with the risk of Alzheimer's disease. N Engl J Med. 2013;368(2):107–16.
16. Keren-Shaul H, Spinrad A, Weiner A, Matcovitch-Natan O, Dvir-Szternfeld R, Ulland TK, et al. A unique microglia type associated with restricting development of Alzheimer's disease. Cell. 2017;169(7):1276–1290.e17.
17. Ulland TK, Colonna M. TREM2 - a key player in microglial biology and Alzheimer disease. Nat Rev Neurol. 2018;14(11):667–75.
18. Zhao N, Liu CC, Qiao W, Bu G, Apolipoprotein E. Receptors, and modulation of Alzheimer's disease. Biol Psychiatry. 2018;83(4):347–57.
19. Shirotani K, Hori Y, Yoshizaki R, Higuchi E, Colonna M, Saito T, et al. Aminophospholipids are signal-transducing TREM2 ligands on apoptotic cells. Sci Rep. 2019;9(1):7508.
20. Konishi H, Kiyama H. Microglial TREM2/DAP12 signaling: a double-edged sword in neural diseases. Front Cell Neurosci. 2018;12:206. https://doi.org/10.3389/fncel.2018.00206.
21. Mecca C, Giambanco I, Donato R, Arcuri C. Microglia and aging: the role of the TREM2-DAP12 and CX3CL1-CX3CR1 axes. Int J Mol Sci. 2018;19(1):318.
22. Zhou Y, Ulland TK, Colonna M. TREM2-dependent effects on microglia in Alzheimer's disease. Front Aging Neurosci. 2018;10:202.
23. Yao H, Coppola K, Schweig JE, Crawford F, Mullan M, Paris D. Distinct signaling pathways regulate TREM2 phagocytic and NFκB antagonistic activities. Front Cell Neurosci. 2019;13:457.
24. Imai Y, Ibata I, Ito D, Ohsawa K, Kohsaka S. A novel gene iba1 in the major histocompatibility complex class III region encoding an EF hand protein expressed in a monocytic lineage. Biochem Biophys Res Commun. 1996;224(3):855–62.
25. Korzhevskii DE, Kirik OV. Brain microglia and microglial markers. Neurosci Behav Physiol. 2016;46:284–90.
26. Shukla AK, McIntyre LL, Marsh SE, Schneider CA, Hoover EM, Walsh CM, et al. CD11a expression distinguishes infiltrating myeloid cells from plaque-associated microglia in Alzheimer's disease. Glia. 2019;67(5):844–56.
27. Hansen DV, Hanson JE, Sheng M. Microglia in Alzheimer's disease. J Cell Biol. 2018;217(2):459–72.
28. Hopperton KE, Mohammad D, Trépanier MO, Giuliano V, Bazinet RP. Markers of microglia in post-mortem brain samples from patients with Alzheimer's disease: a systematic review. Mol Psychiatry. 2018;23(2):177–98.
29. Gudi V, Gai L, Herder V, Tejedor LS, Kipp M, Amor S, et al. Synaptophysin is a reliable marker for axonal damage. J Neuropathol Exp Neurol. 2017;76(2):109–25.
30. Deczkowska A, Keren-Shaul H, Weiner A, Colonna M, Schwartz M, Amit I. Disease-associated microglia: a universal immune sensor of neurodegeneration. Cell. 2018;173(5):1073–81.
31. Zhou Y, Song WM, Andhey PS, Swain A, Levy T, Miller KR, et al. Human and mouse single-nucleus transcriptomics reveal TREM2-dependent and TREM2-independent cellular responses in Alzheimer's disease. Nat Med. 2020;26(1):131–42.
32. Song WM, Colonna M. The identity and function of microglia in neurodegeneration. Nat Immunol. 2018;19(10):1048–58.
33. Tzioras M, Daniels MJD, King D, Popovic K, Holloway RK, Stevenson AJ, et al. Altered synaptic ingestion by human microglia in Alzheimer's disease. bioRxiv 795930. 2019. https://doi.org/10.1101/795930.
34. Jiang T, Zhang YD, Gao Q, Ou Z, Gong PY, Shi JQ, et al. TREM2 ameliorates neuronal tau pathology through suppression of microglial inflammatory response. Inflammation. 2018;41(3):811–23.
35. Lee CYD, Daggett A, Gu X, Jiang LL, Langfelder P, Li X, et al. Elevated TREM2 gene dosage reprograms microglia responsivity and ameliorates pathological phenotypes in Alzheimer's disease models. Neuron. 2018;97(5):1032–1048.e5.
36. Ren M, Guo Y, Wei X, Yan S, Qin Y, Zhang X, et al. TREM2 overexpression attenuates neuroinflammation and protects dopaminergic neurons in experimental models of Parkinson's disease. Exp Neurol. 2018;302:205–13.

37. Zhong L, Wang Z, Wang D, Wang Z, Martens YA, Wu L, et al. Amyloid-beta modulates microglial responses by binding to the triggering receptor expressed on myeloid cells 2 (TREM2). Mol Neurodegener. 2018;13(1):15.
38. Liu W, Taso O, Wang R, Bayram S, Graham AC, Garcia-Reitboeck P, et al. Trem2 promotes anti-inflammatory responses in microglia and is suppressed under pro-inflammatory conditions. Hum Mol Genet. 2020;29(19):3224–48.
39. Filipello F, Morini R, Corradini I, Zerbi V, Canzi A, Michalski B, et al. The microglial innate immune receptor TREM2 is required for synapse elimination and normal brain connectivity. Immunity. 2018;48(5):979–991.e8.
40. Braak H, Braak E. Neuropathological stageing of Alzheimer-related changes. Acta Neuropathol. 1991;82(4):239–59.
41. Folstein MF, Folstein SE, McHugh PR. "Mini-mental state". A practical method for grading the cognitive state of patients for the clinician. J Psychiatr Res. 1975;12(3):189–98.
42. Franklin W, Taglialatela G. A method to determine insulin responsiveness in synaptosomes isolated from frozen brain tissue. J Neurosci Methods. 2016;261:128–34.
43. Marcatti M, Fracassi A, Montalbano M, Natarajan C, Krishnan B, Kayed R, et al. Aβ/tau oligomer interplay at human synapses supports shifting therapeutic targets for Alzheimer's disease. Cell Mol Life Sci. 2022;79:222.
44. Györffy BA, Kun J, Török G, Bulyáki É, Borhegyi Z, Gulyássy P, et al. Local apoptotic-like mechanisms underlie complement-mediated synaptic pruning. Proc Natl Acad Sci U S A. 2018;115(24):6303–8.
45. Gylys KH, Fein JA, Wiley DJ, Cole GM. Rapid annexin-V labeling in synaptosomes. Neurochem Int. 2004;44(3):125–31.

SUPPORTING INFORMATION

Additional supporting information can be found online in the Supporting Information section at the end of this article.

How to cite this article: Fracassi A, Marcatti M, Tumurbaatar B, Woltjer R, Moreno S, Taglialatela G. TREM2-induced activation of microglia contributes to synaptic integrity in cognitively intact aged individuals with Alzheimer's neuropathology. Brain Pathology. 2023;33(1):e13108. https://doi.org/10.1111/bpa.13108